ACS APPLIED MATERIALS & INTERFACES

Research Article

www.acsami.org

An Insight into the Role of Oxygen Vacancy in Hydrogenated TiO_2 Nanocrystals in the Performance of Dye-Sensitized Solar Cells

Ting Su,[†] Yulin Yang,*[,†] Yong Na,[†] Ruiqing Fan,*[,†] Liang Li,[†] Liguo Wei,[†] Bin Yang,[‡] and Wenwu Cao[‡,§]

[†]Department of Chemistry and [‡]Condensed Matter Science and Technology Institute, Harbin Institute of Technology, Harbin 150001, P. R. China

[§]Materials Research Institute, The Pennsylvania State University, University Park, Pennsylvania 16802, United States

Supporting Information

ABSTRACT: Hydrogenated titanium dioxide (H-TiO_2) nanocrystals were successfully prepared via annealing TiO_2 in H_2/N_2 mixed gas flow at elevated temperatures ranging from 300 to 600 °C. Electron paramagnetic resonance (EPR) spectra were used to determine the produced oxygen vacancy in H-TiO_2. Variations in temperature were studied to investigate the concentration change of oxygen vacancy in H-TiO_2. The H-TiO_2 nanocrystals prepared at different temperatures were employed into photoanodes sensitized by N719 dye and found to have exceptional effect on the solar-to-electric energy conversion efficiency (η). Photoanodes with H-TiO_2 nanocrystals hydrogenated at 300 °C show the highest short-circuit current density (J_{sc}) of 18.92 mA cm^{-2} and photoelectrical conversion efficiency of 7.76% under standard AM 1.5 global solar irradiation, indicating a 27 and 28% enhancement in J_{sc} and η, respectively, in comparison to those with TiO_2. The enhancement is attributed to high donor density, narrow band gap and positive shift of flat band energy (V_{fb}) of H-TiO_2 that promote the driving force for electron injection. Intensity-modulated photocurrent spectroscopy (IMPS) accompanied by intensity-modulated photovoltage spectroscopy (IMVS) and other analyses were applied to shed more light on the fundamental mechanisms inside the charge transfer and transport in these systems.

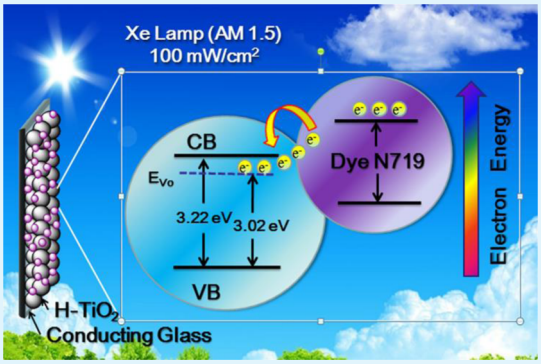

KEYWORDS: *TiO_2 nanocrystals, oxygen vacancy, photoanode, DSSCs, hydrogenation temperature*

INTRODUCTION

Since Grätzel and co-workers developed dye sensitized solar cells (DSSCs) that can convert solar light to electricity, extensive attention have been paid to the nanocrystalline TiO_2-based photoanode in order to improve the device performance and lower the fabrication cost.[1] So far, the TiO_2-based DSSCs have achieved solar-to-electric energy conversion efficiency of 13%[2] and are considered as potential cost-effective alternatives to replace silicon-based devices. Generally, a photoanode is one of the most important ingredients for highly efficient DSSCs, because it can not only function in the loading of dye sensitizers as a pathway for photogenerated electrons transferring into the transparent conductive oxide substrate, but also allow the electrolytes to diffuse in close to the anchored dye molecules.[3−5]

TiO_2 has been widely used in fabrication of photoanodes in DSSC devices, serving as the dye absorbent as well as the medium for electron transport. However, the band gap of 3.0−3.2 eV[6] leads to limitation for its visible-light harvesting and the fast recombination of photogenerated electron/hole pairs.[7] To deal with the above issues, considerable approaches such as metals[8] or nonmetal elements[9,10] doping, shape, and size controlling[11−16] and defects introduction into TiO_2 nanocrystals[17−20] have been developed. Recently, hydrogenation has emerged as a novel approach to effectively modify the properties of materials, which has been able to introduce dramatic structural changes in TiO_2,[21−30] improve its optical, photocatalytic,[26−31] and electronic properties,[26−31] and enhance the lithium-ion storage capability[17,18,32−34] as well as field emission.[35] The high donor density of hydrogenated TiO_2 (H-TiO_2) convinces that it can be an effective method to improve performance of TiO_2 photoanodes in DSSCs with introduction of oxygen vacancies and hydrogen impurities as shallow donors. Furthermore, first-principle calculations on the basis of time-dependent density functional theory show that the oxygen vacancy defects on TiO_2 could improve stabilization of dye adsorption and facilitate charge injection.[36] Moreover, enhanced photovoltaic effect can be observed in solar cells employing H-TiO_2 as photoanode in the absence of any dye.[37] These performances of TiO_2-based electrodes could be suitable for DSSCs. Chen et al. engineered a black TiO_2 prepared by hydrogenation treatment under high pressure H_2 atmosphere for 5 days at 200 °C, which exhibited spectral responses even under infrared light.[27] Besides, the hydrogenated TiO_2 demonstrated high photocatalytic activity because of its surface disordered layer because of the hydrogenation. These ideas

Received: December 4, 2014
Accepted: January 26, 2015
Published: January 26, 2015

DOI: 10.1021/am5085447
ACS Appl. Mater. Interfaces 2015, 7, 3754−3763

stimulated us to incorporate of hydrogenated TiO_2 into solar cell devices and investigate the effect of a hydrogenated TiO_2-based photoanode on the performance of DSSCs.

In this study, hydrogenated TiO_2 was prepared by hydrogen thermal treatment in mixed gas flow with low concentration of hydrogen atmosphere at low temperature and mild pressure, which is different from the strict method reported by Chen et al.[27] And the temperature was employed to investigate the concentration variation of oxygen vacancy in TiO_2 resulted from the hydrogenation. To the best of our knowledge, the application of H-TiO_2 in DSSCs is scarcely reported, and systematical research on the relationship between oxygen vacancy in TiO_2 and the solar energy conversion efficiency of DSSC has not been explored. In comparison with early findings reported,[37,38] a series of concentration of oxygen vacancy in TiO_2 were studied through variations in temperature in order to obtain the practical application of H-TiO_2 in DSSCs. The DSSC devices with hydrogenated TiO_2-based photoanodes indeed enhanced the performances of solar cells and obtain a high photoelectrical conversion efficiency of 7.76%.

EXPERIMENTAL SECTION

Reagents and Materials. Titanium isopropoxide (98%) was obtained from Alfa Aesar and used as received. Pluronic F127, an organic template (Ethylene Oxide/Propylene Oxide Block Copolymer) was purchased from Sigma-Aldrich and used as received. The FTO substrate (90% transmittance in the visible, 15 Ω per square, purchased from NSG, Japan) was used as received. The used Ru complex dye was cis-bis (isothiocyanato)-bis (2,20-bipyridyl-4,40-dicarboxylato) ruthenium(II) bistetrabutylammonium (known as N719, Solaronix Company, Switzerland). The redox electrolyte was consisted of LiI (anhydrous, 99%, Acros), I_2 (99.8%, A. R.), *tert*-butylpyridine (99%, Aldrich) and 1-propyl-2, 3-dimethylimidazolium iodide (99%, A. R.) in 3-methoxypropionitrile (99%, Fluka). In the experiments, all of the chemicals agents and solvents used were reagent grade without further purification.

Synthesis of Hydrogenated TiO_2. The TiO_2 nanopowders were prepared via a facile sol−gel hydrothermal method modified from Chen et al.[33] 0.03 M titanium isopropoxide was added dropwise into mixture of 60 mL deionized water, 0.4 mL HNO_3 and a solution of 2 g of organic template pluronic F127 in water under vigorous stirring. After this step was accomplished, the mixture was stirred at 90 °C for about 5 h to obtain gel-like mixture. The obtained mixture was transferred into a sealed Teflon-lined autoclave and kept at 200 °C for 24 h. After the reaction was completed, the resultant product was washed three times with DI water and absolute ethanol before drying at 80 °C for 6 h and subsequently calcined at 450 °C for 30 min to obtain the white TiO_2 powders.

The obtained TiO_2 were placed in the quartz boat and heated in tube furnace under a 400 sccm mixture gas flow of 10% H_2 and 90% N_2 for 5 h at 300, 400, 500, and 600 °C, respectively. The heating of the hydrogen thermal treatments was stepped at 1 °C min^{-1}. After the hydrogen thermal treatment, the sample powders were maintained in a vacuum for 1 h for stabilization.

Devices Fabrication. Dye-sensitized solar cells were fabricated according to the following procedures which is similar to our previous work.[39] TiO_2 paste was prepared by mixing TiO_2 nanopowders and ethyecellulose in α-terpinol (wt % ratio: 16.8:4.5:78.7). By screen-printing method prepared TiO_2 paste was cast onto the FTO substrate, and then the electrode was dried at 120 °C for 5 min. This procedure was repeated for six times. After sintering the electrode at 450 °C for 20 min in the air, a transparent TiO_2 electrode with the thickness of ca.10 μm was obtained. H_2PtCl_6 paste was deposited onto the FTO glass substrates and then calcined at 450 °C for 30 min to obtain the platinum counter electrode. The prepared mesoporous TiO_2 electrode was dye-coated by immersing into a 0.3 mM N719 dye solution in absolute ethanol for 20 h. The electrolyte was injected between the dye sensitized photoanode and the counter electrode, and then the cells were assembled held together with clips on the basis of sandwich-type cell. The electrolyte applied in this work was 0.5 M LiI, 0.05 M I_2, 0.1 M *tert*-butylpyridine in acetonitrile-propylene carbonate mixture.

Characterization. The X-ray powder diffraction (XRD) measurement was analyzed with Cu−Kα radiation by Shimadzu XRD-6000 X-ray Diffraction instrument. Scanning electron microscope (SEM) micrographs were performed by Rili SU 8000HSD Series Hitachi New Generation Cold Field Emission SEM. Transmission electron microscopy (TEM) experiment was performed on an electron microscope (H-7650, Japan) using an acceleration voltage of 80 kV. UV−visible absorption spectra of TiO_2 films were recorded on a Japan Shimadzu model UV-2250 spectrophotometer. X-ray photoelectron spectroscopy (XPS) was performed with ESCALAB-250 spectrometer (Thermo, America) using an Al−Kα source and working in an ultrahigh vacuum (UHV) at 3.5×10^{-7} Pa. EPR spectra were registered at 300 K using a Bruker ER083CS spectrometer, at a microwave frequency of 9.85 GHz. Photocurrent-photovoltage (I−V) curves were recorded by CHI660D electrochemical potentiostat. The AM 1.5 global sunlight intensity was calibrated by a standard Si solar cell (NO. NIMMS1123, calibrated at National Institute of Metrology, P. R. China) from a filtered 500 W xenon lamp with an AM 1.5 global filter from Newport. Electrochemical impedance spectra (EIS) were recorded using CHI660D electrochemical potentiostat. The measurements were obtained over a frequency range of 0.1−100 kHz under standard AM 1.5 global solar irradiation conditions or in the dark. The Mott−Schottky analysis were performed at f = 200 Hz with a small amplitude of 10 mV by CHI660D electrochemical potentiostat using a three electrode cell with a platinum wire as counter electrode and a standard Ag/AgCl as reference electrode. The supporting electrolyte used in Mott−Schottky analysis was 0.01 M $LiClO_4$, 0.1 M LiI and 1 mM I_2. The Incident Photon-to-Current Efficiency (IPCE) spectra were conducted by IPCE Kit equipment (Oriel, U.S.A.). IMPS and IMVS (Zahner Elektrik, Germany) were applied to analyze the electron transport and recombination properties. The DSSCs were probed by a frequency response analyzer through the photoanode side applying a white light-emitting diode (wlr-01). The frequency range was 0.1−1000 Hz and the irradiated intensity was varied from 30 to 150 mW cm^{-2}.

RESULTS AND DISCUSSION

Morphology and Crystal Structure Analysis. Figure 1 shows the X-ray structural analysis of the TiO_2 and hydrogenated TiO_2. All plots demonstrate that the prepared samples before and after hydrogen thermal treatment possess the same

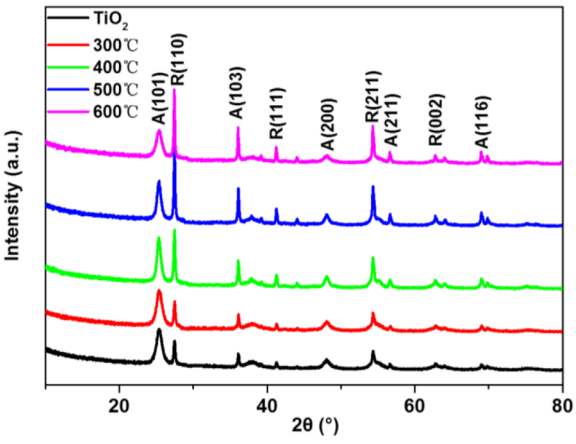

Figure 1. XRD spectra collected for TiO_2 samples before and after hydrogen treatment. Diffraction peaks for anatase (JCPDS#21−1272) and rutile (JCPDS#21−1276) are labeled with A (*hkl*) and R (*hkl*), respectively.

DOI: 10.1021/am5085447
ACS Appl. Mater. Interfaces 2015, 7, 3754−3763

crystalline structure, which are mixed phases including anatase (JCPDS#21−1272) and rutile (JCPDS#21−1276). The hydrogenated TiO_2 samples treated under high temperature show stronger peak intensity of rutile (110) peak at $2\theta = 27.4°$ in the order of TiO_2 < 300 °C H-TiO_2 < 400 °C H-TiO_2 < 500 °C H-TiO_2 < 600 °C H-TiO_2, implying an increment of the ratio of rutile after hydrogenation. Content of rutile by XRD (%) is estimated from the respective integrated XRD peak intensity using the following equation: $\chi = (1 + 0.8I_A/I_R)^{-1}$.[40,41] The results of five samples in our work are as follows: rutile content of TiO_2, 300 °C H-TiO_2, 400 °C H-TiO_2, 500 °C H-TiO_2, and 600 °C H-TiO_2 is 45.2, 44.4, 55.9, 62.7, and 65.2%, respectively. The increasing content of rutile may induce the low photoelectrochemical performance. This result is in accordance with early reports, which showed the anatase to rutile phase transition[42] occurs upon annealing above 550 °C.[27] In the O-rich regime, the temperature of anatase to rutile phase transformation is higher than 700 °C, reduction conditions of hydrogen thermal environment is more feasible to induce the phase transition.

The morphology of the TiO_2 and H-TiO_2 treated at 300 °C was analyzed by SEM in Figure S1 (Supporting Information). It can be seen that there is no obvious difference in the nanoparticles morphology before and after hydrogen thermal treatment. TiO_2 and H-TiO_2 treated at 300 °C are selected as the representative samples. Most of them are nano sized particles with small amount of V shape crystals. The TEM micrographs of hydrogenated H-TiO_2 treated at 300 °C are shown in Figure 2a, which reveals the crystallite size to be about

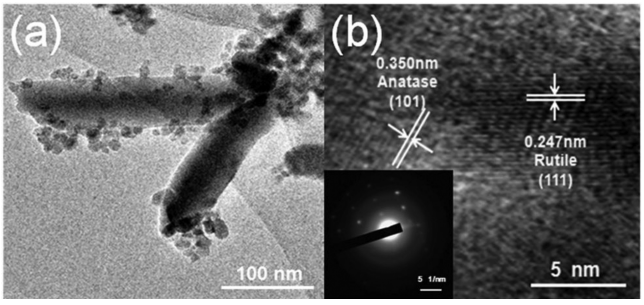

Figure 2. (a) TEM images of hydrogenated TiO_2 treated at 300 °C and (b) high-resolution TEM images of TiO_2 correlating to the (101) and (111) interplanar crystal spacing.

10 nm, and the edge length of V shape crystallite is closed to 300 nm. The well-defined surface edges of the H-TiO_2 treated under 300 °C (in Figure 2b) become disordered after hydrogenation, clearly confirming that the TiO_2 matrix sample owns both anatase and rutile phases. The interplane spacing of the TiO_2 and H-TiO_2 samples are identical and found to be 0.350 and 0.247 nm for anatase and rutile phases, respectively. The SAED pattern (Inset Figure 2b) shows that the particles are crystalline in nature.

XPS was further utilized to determine the transformation of surface chemical bonding environment and explore the electronic valence band position of these TiO_2 samples. As indicated in Figure S3a in the Supporting Information, the XPS survey spectra illustrate that all the samples display similar features, indicating that the mixed gas flow treatment including nitrogen and hydrogen does not introduce impurities. Figure S3c in the Supporting Information demonstrates that Ti 2p of the samples in core-level XPS spectra own similar features. The TiO_2 nanocrystals possess typical Ti^{4+} features with Ti $2p_{3/2}$ peak centered at 458.4 eV and Ti $2p_{1/2}$ peak centered at 464.1 eV. None of additional shoulder peak centered at 457.0 eV indicates the absence of Ti^{3+} ions.[27] The O 1s core-level XPS spectra (Figure S3d in the Supporting Information) show that all the samples have similar O 1s peaks centered at 529.7 eV, suggesting similar oxygen environments. As temperature elevated, the O 1s peaks exhibit an increasing stronger shoulder peak around high binding energy compared with the TiO_2. The O 1s shoulder peak can be ascribed to the chemisorbed O_2, which can accept electrons from oxygen vacancies, indicating the concentration of oxygen vacancies in H-TiO_2 under different temperature. The O 1s region illustrates the presence of three components attributed to O−Ti (O_{Ti}), a surface OH group (O_{OH}), and O−C (O_C).[43] As is shown in Table S1 in the Supporting Information, the estimated atom percentages (at. %) of O_{Ti} peaks decreases with the enhancement of temperature, O_{OH} of H-TiO_2 treated under 600 °C increases approximately 43.8% compared to that of TiO_2. The improvement means H-TiO_2 samples have more surface OH species produced by the O and H interaction, thus indicating oxygen vacancy concentration introduced by hydrogen thermal treatment increases with the hydrogen thermal treatment to some extent.[38] The effect of hydrogen thermal treatment on the electronic band structure of TiO_2 can be provided by the valence band spectra of both the TiO_2 and H-TiO_2 nanopowders using XPS. As shown in Figure 3, the valence band

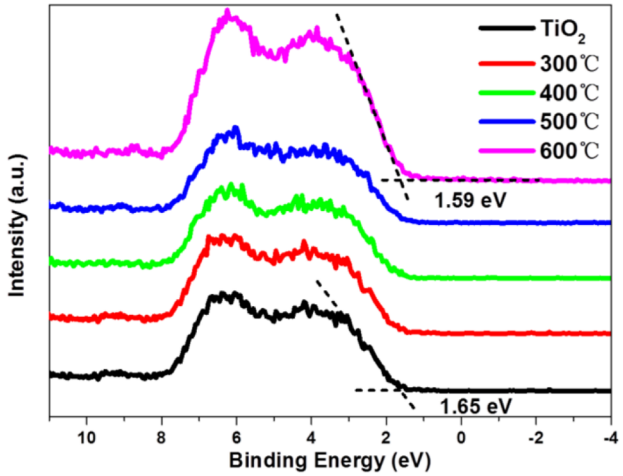

Figure 3. Valence band of TiO_2 and H-TiO_2 treated under different temperatures.

spectra of TiO_2 and H-TiO_2 nanopowders are similar. Linear extrapolation of the peaks to the baselines can be employed to estimate the valence band maxima of samples, which produce band edge positions of 1.65 and 1.59 eV below the Fermi energy for TiO_2 and H-TiO_2 treated at 600 °C. The relative low temperature has slight effect on the valence band values, which is likely due to that the disorders and defects generate some localized states above the valence band edge and finally result in the band gap narrowing.

EPR was applied to detect unpaired electrons in paramagnetic species, which is the powerful method to certify the existence of Ti^{3+} and oxygen vacancies. EPR spectra were registered at 300 K using a Bruker ER083CS spectrometer, at a microwave frequency of 9.85 GHz and the same quality TiO_2 powders samples were charged in quart glass tubes connected

DOI: 10.1021/am5085447
ACS Appl. Mater. Interfaces 2015, 7, 3754−3763

to N_2 gas. Figure 4 displays the EPR spectra measured at 300 K of all samples without light illumination. No signal can be

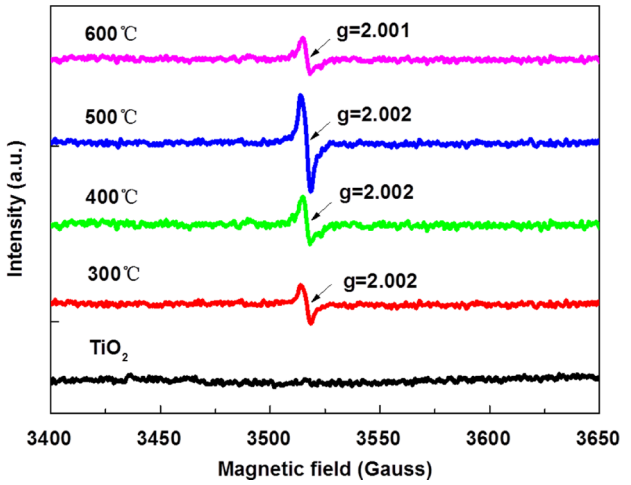

Figure 4. EPR spectra recorded at 300 K for TiO_2, H-TiO_2 samples.

detected for TiO_2, indicating free of paramagnetic species existing in TiO_2. In contrast, apparent symmetrical signals at g = 2.002 and g = 2.001 appear in the EPR spectra of H-TiO_2 samples, which can be attributed to the defects like oxygen vacancy (with one electron) in H-TiO_2.[44] The above results certificate the existence of oxygen vacancy in H-TiO_2. Furthermore, the intensity of the signals for H-TiO_2 samples in EPR spectra increases as the treated temperature rising. The EPR signal gained the relative strongest value at 500 °C, however, when the treatment temperature was further elevated to 600 °C the signal intensity declines, indicating that the density of oxygen vacancy reaches saturation point on the surface of H-TiO_2 at 500 °C.

The spectral responses of hydrogenated TiO_2 enhanced in the visible region from 250 to 750 nm are shown in Figure 5, which indicates the existence of oxygen vacancy affect the light absorption properties of TiO_2. All samples demonstrate a sharp increase in the absorbance before 400 nm, which is originated from anatase TiO_2. The samples at 500 and 600 °C expand the absorption edge of TiO_2 in UV−visible range with slightly red-shift. From the Tauc plot The band gaps of the TiO_2 and H-TiO_2 can be calculated, a relationship between the absorption coefficient (α) near the absorption edge and the optical band gap (E_g), as shown in the equation: $(\alpha h\nu)^2 = A(h\nu - E_g)$, where α is absorption coefficient, h stands for Planck's constant, ν represents the frequency of light vibration, A is the proportional constant, and E_g is the band gap,[45] plots of $(\alpha h\nu)^2$ vs $h\nu$ are shown in Figure S2 in the Supporting Information. The relationship between the temperature and the band gap is shown in Figure 5b, illustrating band gap value decreasing with treated temperature. Band gap value of 600 °C H-TiO_2 is 3.02 eV, which is narrower than that of TiO_2 (3.22 eV), resulting in its light-absorption toward red shift. The hydrogenation had little effect on the band gap value, whereas H-TiO_2 samples exhibited a remarkable absorption in the visible light region. The strong absorption band can be attributed to the low-energy photon of trapped electron in localized below the conduction band minimum to the conduction band. The white color of TiO_2 was changed to light yellow after hydrogenation at low temperature (300−400 °C), and then to a bit darker gray at 600 °C (Figure 5b).

Mott−Schottky analysis of impedance was conducted to investigate the electronic properties influenced by hydrogen thermal treatment on the TiO_2 samples. As shown in Figure 6,

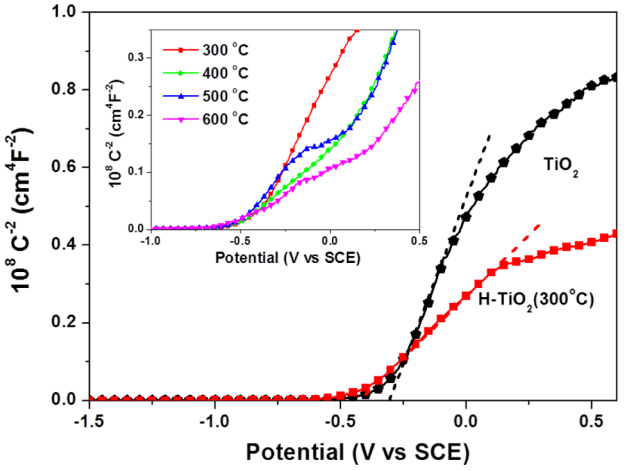

Figure 6. Mott−Schottky plots collected in the dark for the TiO_2 and the H-TiO_2 nanopowders. Inset Figure: Mott−Schottky plots of H-TiO_2 nanopowders prepared at 300, 400, 500, and 600 °C, which was collected under the same conditions.

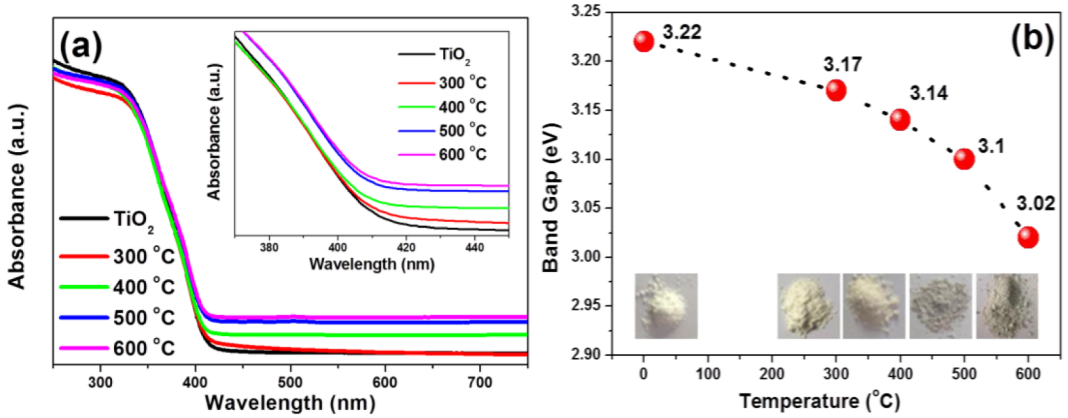

Figure 5. (a) UV−vis spectra of TiO_2 and H-TiO_2 samples, inset figure is the partial enlarged drawing of a; (b) band gap energy at different temperature, inset figure is color variation of TiO_2 and H-TiO_2 samples at different temperature.

DOI: 10.1021/am5085447
ACS Appl. Mater. Interfaces 2015, 7, 3754−3763

positive slopes convince that all samples are n-type semiconductor and hydrogen treatment has no effect on transition in type of semiconductor. The H-TiO_2 nanoparticles show smaller slopes compared to the TiO_2 sample, indicating higher donor densities. Donor densities can be estimated from Mott–Schottky plots using the following equation

$$N_d = \left(\frac{2}{e_0 \varepsilon \varepsilon_0}\right)\left(\frac{d\frac{1}{C^2}}{dV}\right)^{-1}$$

Where N_d is the donor density, e_0 is the electron charge, ε is the dielectric constant of TiO_2 (ε = 170), ε_0 is the permittivity of vacuum, and V is the applied bias at the electrode. According to this equation, the donor densities of the TiO_2 and H-TiO_2 nanopowders treated at 300 °C were 2.70 × 10^{21} and 3.53 × 10^{21} cm^3, respectively. The enhanced donor density in H-TiO_2 could improve the charge transport in the TiO_2 nanoparticles, resulting in enhanced charge collection efficiency. By comparing these slopes derived from the Mott–Schottky plots qualitatively, the smaller slope of H-TiO_2 sample leads to enhancement of carrier density in H-TiO_2. The enhanced donor density is originated from the increased oxygen vacancy, which is known as electron donors for TiO_2.[46] The increased donor density improves not only the charge transport in TiO_2 samples after hydrogenation but also the interface electron transfer between the nanopowders and the FTO substrate. On the other hand, after hydrogen thermal treatment, the increased electron density is responsible for the downward-shift of Fermi level of TiO_2 toward the conduction band, which facilitates the charge separation at the TiO_2/electrolyte interface.[47] The enhanced charge separation and transportation are determined to be the dominant factor for the obtained IPCE enhancement in the UV region,[32] on the other hand, the surface defect introduction from oxygen vacancy could increase the trap state density along with the elevated temperature to some extent and increase the electron–hole recombination loss.[48] When the donor density reaches to certain saturation, the electron–hole recombination becomes a crucial element decreasing the efficiency of electron collection.

During electron injection process, not only the different positions of the excited energy level of the dye but also the conduction band minimum of the TiO_2 are of great importance. Spectro-electrochemical measurements[49,50] and Mott–Schottky analyses[51] are commonly employed to evaluate the V_{fb}, which are essential to elucidate the band energy of semiconductor electrode. In this work, the Mott–Schottky analyses were used to gain the V_{fb} of TiO_2 and H-TiO_2. The result in Figure 6 indicates a positive shift of V_{fb} due to the existence of oxygen vacancy after hydrogen thermal treatment. In addition, the tendency is presented in inset figure indicating that as temperature elevated, the V_{fb} shift positively. The driving force of electron injection derived from the difference value between flatband energy (E_{fb}) of TiO_2 and the LUMO of the dye,[52] accordingly is boosted by hydrogen thermal treatment, which is beneficial for the enhanced efficiency of the electron-injection.

It is obvious that the narrowed band gap, the downward-shift of Fermi level, the enhanced donor density and other particular characteristics of H-TiO_2 are closely related to the existence of oxygen vacancy because of hydrogen thermal treatment. Hydrogen thermal treatment alters the location of oxygen vacancy levels, which are situated about 0.75–1.18 eV lower than the conduction band of TiO_2;[53] as illustrated in Figure 7, E_{Vo} located below the TiO_2 conduction band represents the energy level of oxygen vacancy. The introduced oxygen vacancy could downward-shift Fermi level, which leads to the increase of donor density and the narrowed band gap. This downward-shift of the Fermi level is responsible for the reduction of the TiO_2 work function,[35] which may be conducive to the photoelectronchemical performance. It can be concluded that there is a balanced point where appropriate oxygen vacancies make the electrons transport faster than TiO_2 and bring the recombination and transportation into balance, which can make photoelectronchemical performance better. Besides, the introduced oxygen vacancy in H-TiO_2 by hydrogen thermal treatment will improve their conductivity and carrier mobility, which can boost most injected electrons transportation in H-TiO_2.[35] It is considered that only the existence of an appropriate quantity concentration of oxygen vacancies could ensure that H-TiO_2 samples exhibit excellent photoelectronchemical performance, and this work keeps close watch on this target to find the appropriate condition.

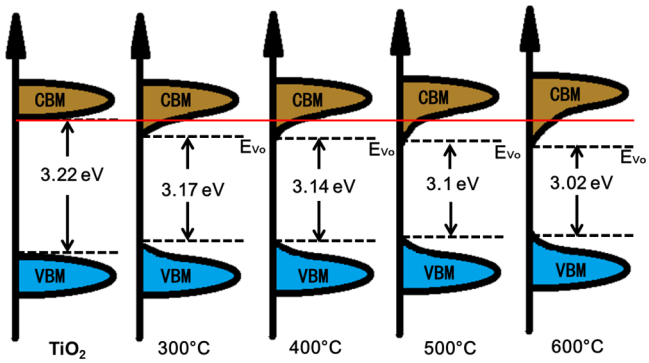

Figure 7. Schematic diagrams of electronic band structure of TiO_2 and H-TiO_2. E_{Vo} located below the TiO_2 conduction band represents the energy levels of oxygen vacancy.

Photoelectrochemical Performance of Dye-Sensitized Solar Cells. The photoelectrochemical measurement was recorded under standard AM 1.5 global solar irradiation conditions and each value was taken as an average of five samples. The typical photocurrent–photovoltage curves of TiO_2 and the H-TiO_2 based DSSCs are shown in Figure 8 and detailed photovoltaic parameters of DSSCs with different hydrogen thermal treatment are shown in Table S2 in the Supporting Information. To reduce error and convince the reproducibility of our experiments, we collected relative experimental data and calculated carefully.[54] The amount of dye-loading of photoanodes based on H-TiO_2 was tested (see Table S2 in the Supporting Information). Comparing photoanodes based on H-TiO_2 treated at 300 °C with photoanodes based on H-TiO_2, there are no indications of any great change in the amount of dye-loading eliminating the adsorption effect on accurate conclusion. As the temperature elevated, the amount of dye-loading indicates a sharp decrease, which may induce the low efficiency of DSSCs. The DSSCs based on H-TiO_2 shows a J_{sc} of 18.92 mA cm^{-2} and a V_{oc} of 0.72 V, corresponding to overall conversion efficiency of η as 7.76%, whereas the DSSCs based on TiO_2 gives a J_{sc} of 14.88 mA cm^{-2} and a V_{oc} of 0.70 V, corresponding to overall conversion efficiency of η as 6.07%, indicating a 27 and 28% increase in J_{sc} and η, respectively. The DSSCs based on pure hydrogenated

DOI: 10.1021/am5085447
ACS Appl. Mater. Interfaces 2015, 7, 3754–3763

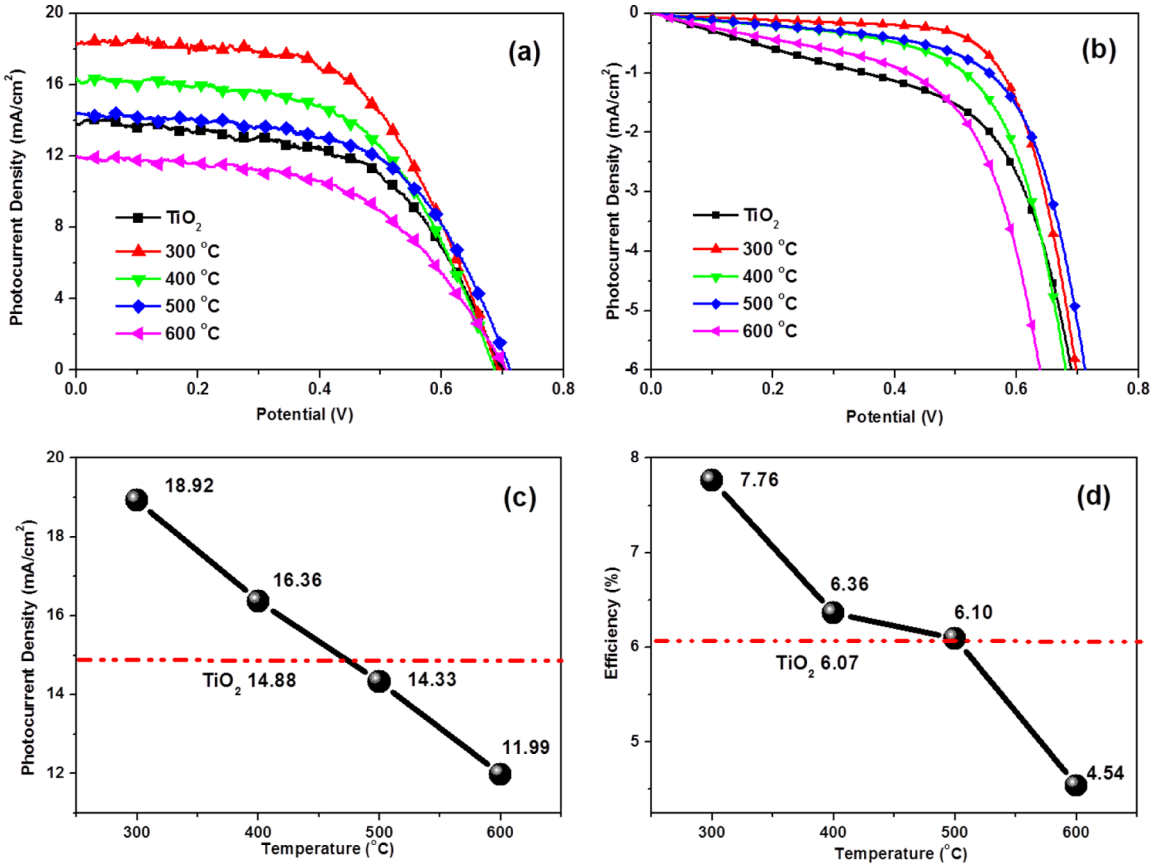

Figure 8. Photocurrent−photovoltage curves (a) under illumination and (b) in the dark of the DSSCs based on TiO_2 and H-TiO_2 hydrogen thermal treated at 300, 400, 500, and 600 °C.

anatase and rutile samples were measured and the results are listed in Table S2 in the Supporting Information. The increasing rutile content of samples can also lead to the declining conversion efficiency of DSSCs.[55] The dark current of the DSSCs depends on the recombination of injected electron with I_3^- in the electrolyte. The photocurrent−photovoltage curves of DSSCs based on TiO_2 and the H-TiO_2 nanopowders in the dark are shown in Figure 8b. The dark curves indicate that the hydrogen-treated DSSCs exhibit lower recombination rate, which could improve the efficiency of the device.[17]

Figure 8c, d show the trend of J_{sc} and η of different DSSCs. It is obvious that DSSCs based on H-TiO_2 at 300 °C achieve the highest J_{sc} of 18.92 mA cm^{-2} and η of 7.76%. The J_{sc} for DSSCs based on H-TiO_2 at 300 and 400 °C are 18.92 mA cm^{-2} and 16.36 mA cm^{-2}, respectively, which are higher than that based on TiO_2. However, as the temperature for hydrogenation higher than 400 °C, the J_{sc} for DSSCs based on H-TiO_2 decreased. And what's more, the η values for DSSCs based on TiO_2 and H-TiO_2 at different temperatures show the same tendency, in which the highest η of 7.76% is achieved with the device based on H-TiO_2 at 300 °C. The improvement in J_{sc} may be due to the enhancement of the electrical conductivity[35] of TiO_2 under the effect of hydrogen thermal treatment, which can be explained by the positive shifted value of V_{fb} in Mott−Schottky analysis.

According to this process, the driving force for electron injection is increased by hydrogen thermal treatment, which correspondingly contributes to the enhanced electron-injection efficiency and higher J_{sc}. The J_{sc} shows a drastic increase in the initial stage and reaches to a saturated state less than 400 °C. The result confirms that the light-absorption property was improved due to the narrowed band gap from UV spectra, which is beneficial for the DSSC performance. What's more, appropriate oxygen vacancy is conducive to enhancing the photoelectrical conversion efficiency performance of DSSCs, and the appropriate oxygen vacancies enhance the electrons transportation from Mott−Schottky analysis and bring the recombination and transportation into balance. After the saturated point of oxygen vacancies, the electron transportation gets hindered to some extent together with faster recombination rate, which lead to the decrease of J_{sc} based on H-TiO_2 compared with J_{sc} based on TiO_2.

The correlationship curves between (c) photocurrent and temperature (d) η and temperature of the DSSCs based on TiO_2 and H-TiO_2 annealed at different temperature of hydrogen treatment.

Figure 9 shows the spectra of IPCE of DSSCs with different photoanodes. IPCE spectra of all samples have similar profiles with high IPCE values in the wavelength region between 350 to 650 nm. Apparently, the DSSC with H-TiO_2 treated at 300 °C shows the highest IPCE value of 80.6%, suggesting the efficient photoexcited charge carriers separation and transport. The values of photoanodes based on H-TiO_2 treated at different temperatures are in the order of 300 °C > 400 °C > 500 °C > TiO_2 > 600 °C, which is in consistent with the decreased order of J_{sc}. EIS has been widely utilized to analyze the electronic and ionic transport processes in an electrochemical device, current response measurement based on the application of an AC voltage at different frequencies can be explained by this steady state method.[56,57] For the purpose of a deep understanding of

DOI: 10.1021/am5085447
ACS Appl. Mater. Interfaces 2015, 7, 3754−3763

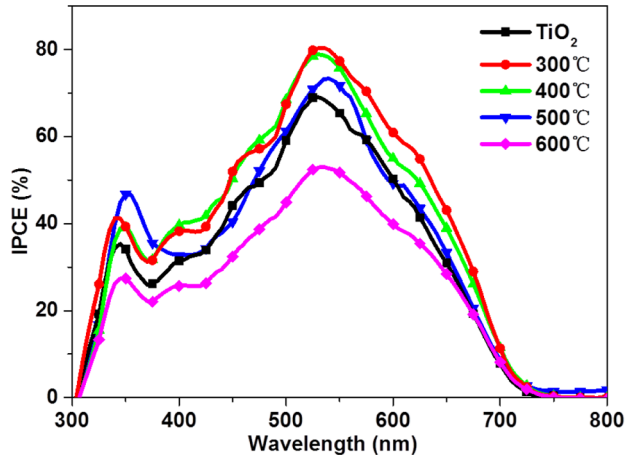

Figure 9. IPCE spectra of DSSCs based on TiO_2 and H-TiO_2 annealed at different temperature.

the complex charge transfer process, a physical model has been proposed,[58,59] and the corresponding parameters obtained by the equivalent circuit are listed in Table S3 in the Supporting Information. As indicated in Figure S5 in the Supporting Information, there are three semicircles in the Nyquist plot with the frequency ranging from 0.1 to 10 kHz. Under the illumination and open circuit voltage condition, the radius of the large semicircle located in middle frequency region in the Nyquist plot represents the charge transfer resistance (R_1). As shown inTable S3 in the Supporting Information, R_1 decrease from 5.19 to 8.18 Ω after TiO_2 was hydrogenated at 300 °C, indicating faster electron transport at the interface of DSSCs based on H-TiO_2. This means that DSSCs devices based on H-TiO_2 is better in electron transportation due to high donor density compared to that based on TiO_2, which is agree with the conclusion from $I-V$ curves.[60,61]

To further elucidate the influences of hydrogen thermal treatment on the photovoltaic parameters, the IMVS and IMPS measurements of DSSCs were employed to investigate the electron transport and charge recombination dynamics under an illumination with different light intensities ranging from 30 to 150 W m^{-2}, there are two important factors to evaluate the performance of DSSCs: the electron recombination time (τ_n), the electron transport time (τ_d), (shown in Figure 10). They are the consequence of the competition between the recombination and transport of electrons across the photoanode. τ_n and τ_d are calculated by IMVS and IMPS measurements through the expression: $\tau_n = (1/2\pi f_n)$ and τ_d $(1/2\pi f_d)$,[62−64] where f_d and f_n are the characteristic frequency minima of the IMVS and IMPS imaginary components, respectively.

The transport time (τ_d) and recombination time (τ_n) of the cells shorten with the increasing light intensity. The recombination time of different samples is shown in Figure 10a. The photoanode based on H-TiO_2 treated at 300 °C shows the longest charge recombination time and the shortest charge transport time, which can reduce the recombination rate of electron and holes, accelerate the mobility of electron and the redox reaction, and enhance the photoelectrical conversion efficiency on the whole. This is in accordance with the aforementioned discussion that the balanced point due to appropriate oxygen vacancy concentration brings the charge recombination and transportation into balance, which can enhance the performance of DSSC devices.

Figure 11 shows the schematic of charge transfer mechanism for DSSCs based on H-TiO_2 under standard AM 1.5 global solar irradiation conditions. The DSSC is based on the photoexcitation of the dye, followed by electron injection into the conduction band of the H-TiO_2 nanoparticle. During light irradiation, the dye absorbs incident light and promotes electrons to the excited state. The excited electrons are injected into the conduction bands of H-TiO_2 nanoparticles. Due to the

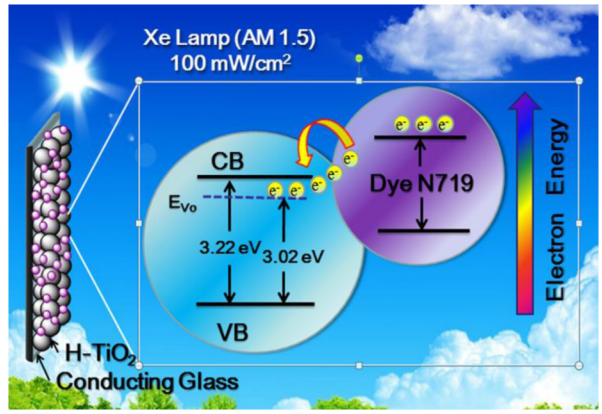

Figure 11. Charge transfer mechanism for photoanode-modified DSSC based on H-TiO_2.

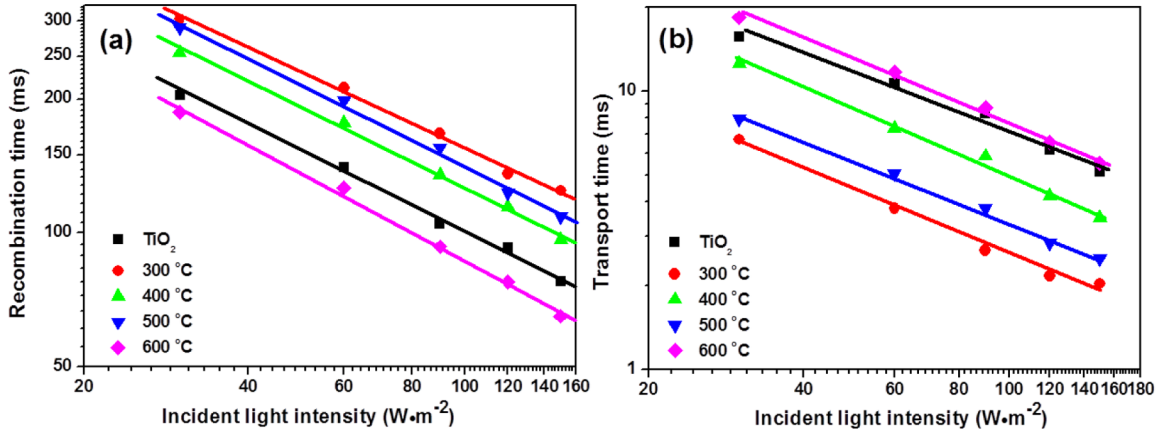

Figure 10. (a) The IMVS response, (b) IMPS response of DSSCs based on TiO_2 and H-TiO_2.

DOI: 10.1021/am5085447
ACS Appl. Mater. Interfaces 2015, 7, 3754−3763

existence of relative low oxygen vacancy energy level, it might be easy for electron transfer from the conduction band of dye N719 to oxygen vacancy energy level, and then electrons move toward the valence band of H-TiO_2. The dye is then reduced by receiving electrons from the electrolyte through the redox system, and is ready to be used again. The H-TiO_2 nanoparticles prepared in this work possess narrow band gap, the downward-shift of Fermi level, the enhanced donor density and other particular characteristics due to the existence of oxygen vacancy from hydrogen thermal treatment. Therefore, a significant enhancement of photocurrent and a relative high solar-to-electric energy conversion efficiency have been achieved.

CONCLUSIONS

In summary, hydrogenated TiO_2 with narrow band gap and high donor density has been fabricated by introducing the oxygen vacancy through hydrogen thermal treatment. The obtained products can not only facilitate the charge transfer process of the photoanodes, but also improve the total performance of DSSC devices. Photoanodes based on H-TiO_2 nanocrystals hydrogenated at 300 °C exhibit significant enhancement of J_{sc} from 14.88 mA cm^{-2} to 18.92 mA cm^{-2} and η 6.07 to 7.76%, respectively. Photoelectrochemical performance is obviously improved via the appropriate concentration of oxygen vacancy, demonstrating that the hydrogenated TiO_2 can act as a good candidate for efficient photoanode materials of DSSCs. Surface-disorder and narrow band gap characteristics of the outer layer in the particles provide an alternative to high performance DSSC materials. It is worthy to note that this newly developed electrode material is prepared only by a simple hydrogen thermal treatment through low cost and easily handled process, which deserves to be explored for the application in DSSCs.

ASSOCIATED CONTENT

Supporting Information

SEM images of TiO_2 samples and hydrogenated TiO_2; Tauc plots of TiO_2 and hydrogenated TiO_2; XPS spectra and atom percentages of the O 1s and Ti 2p peaks determined by the XPS analysis; photoelectric properties of DSSC with different treatment; equivalent circuit used to represent interface in DSSCs consisting of FTO glass substrate/TiO_2/dye/I_3^-/I^-||Pt/FTO glass substrate; parameters obtained by the equivalent circuit. This material is available free of charge via the Internet at http://pubs.acs.org.

AUTHOR INFORMATION

Corresponding Authors

*E-mail: ylyang@hit.edu.cn. Fax: +86-451-86418270.
*E-mail: fanruiqing@hit.edu.cn.

Notes

The authors declare no competing financial interest.

ACKNOWLEDGMENTS

This work was supported by National Natural Science Foundation of China (Grant 21171044 and 21371040), the National key Basic Research Program of China (973 Program, 2013CB632900), and the Fundamental Research Funds for the Central Universities (Grant HIT. IBRSEM. A. 201409), also Program for Innovation Research of Science in Harbin Institute of Technology (PIRS of HIT A201416 and B201414).

REFERENCES

(1) O'Regan, B.; Grätzel, M. A Low-Cost, High-Efficiency Solar Cell Based on Dye-Sensitized Solloidal TiO_2 Films. *Nature* **1991**, *353*, 737−740.
(2) Mathew, S.; Yella, A.; Gao, P.; Humphry-Baker, R.; Curchod, B. F.; Ashari-Astani, N.; Tavernelli, I.; Rothlisberger, U.; Nazeeruddin, M. K.; Grätzel, M. Dye-Sensitized Solar Cells with 13% Efficiency Achieved through the Molecular Engineering of Porphyrin Sensitizers. *Nat. Chem.* **2014**, *6*, 242−247.
(3) Kim, Y. J.; Lee, M. H.; Kim, H. J.; Lim, G.; Choi, Y. S.; Park, N. G.; Kim, K.; Lee, W. I. Formation of Highly Efficient Dye-Sensitized Solar Cells by Hierarchical Pore Generation with Nanoporous TiO_2 Spheres. *Adv. Mater.* **2009**, *21*, 1−6.
(4) Zhang, Q. F.; Park, K.; Xi, J. T.; Myers, D.; Cao, G. Z. Recent Progress in Dye-Sensitized Solar Cells Using Nanocrystallite Aggregates. *Adv. Energy Mater.* **2011**, *1*, 988−1001.
(5) Miao, X.; Pan, K.; Liao, Y.; Zhou, W.; Pan, Q.; Tian, G.; Wang, G. Controlled Synthesis of Mesoporous Anatase TiO_2 Microspheres as a Scattering Layer to Enhance the Photoelectrical Conversion Efficiency. *J. Mater. Chem. A* **2013**, *1*, 9853−9861.
(6) Diebold, U.; Ruzycki, N.; Herman, G. S.; Selloni, A. One Step towards Bridging the Materials Gap: Surface Studies of TiO_2 Anatase. *Catal. Today* **2003**, *85*, 93−100.
(7) Llansola-Portoles, M. J.; Bergkamp, J. J.; Finkelstein-Shapiro, D.; Sherman, B. D.; Kodis, G.; Dimitrijevic, N. M.; Gust, D.; Moore, T. A.; Moore, A. L. Controlling surface defects and photophysics in TiO_2 nanoparticles. *J. Phys. Chem. A* **2014**, *118*, 10631∼1−8.
(8) Zheng, Z.; Huang, B.; Meng, X.; Wang, J.; Wang, S.; Lou, Z.; Wang, Z.; Qin, X.; Zhang, X.; Dai, Y. Metallic Zinc-Assisted Aynthesis of Ti^{3+} Self-Doped TiO_2 with Tunable Phase Composition and Visible-Light Photocatalytic Activity. *Chem. Commun.* **2013**, *49*, 868−870.
(9) Zhang, H. J.; Chen, G.; He, X. D.; Xu, J. Synthesis and Visible Light Photocatalysis Water Splitting Property of Cu-Doped $NaInS_2$ Synthesized by a Hydrothermal Method. *Mater. Res. Bull.* **2012**, *47*, 4483−4486.
(10) Jung, S. M.; Choi, I. T.; Lim, K.; Ko, J.; Kim, J. C.; Lee, J. J.; Ju, M. J.; Kim, H. K.; Baek, J. B. B-Doped Graphene as an Electrochemically Superior Metal-Free Cathode Material As Compared to Pt over a Co(II)/Co(III) Electrolyte for Dye-Sensitized Solar Cell. *Chem. Mater.* **2014**, *26*, 3586−3591.
(11) Yang, H. G.; Sun, C. H.; Qiao, S. Z.; Zou, J.; Liu, G.; Smith, S. C.; Cheng, H. M.; Lu, G. Q. Anatase TiO_2 Single Crystals with a Large Percentage of Reactive Facets. *Nature* **2008**, *453*, 638−641.
(12) Han, X.; Kuang, Q.; Jin, M.; Xie, Z.; Zheng, L. Synthesis of Titania Nanosheets with a High Percentage of Exposed (001) Facets and Related Photocatalytic Properties. *J. Am. Chem. Soc.* **2009**, *131*, 3152−3153.
(13) Wang, Z. Y.; Lv, K. L.; Wang, G. H.; Deng, K. J.; Tang, D. G. Study on the Shape Control and Photocatalytic Activity of High-Energy Anatase Titania. *Appl. Catal., B* **2010**, *100*, 378−385.
(14) Zheng, Z.; Huang, B.; Qin, X.; Zhang, X.; Dai, Y.; Jiang, M.; Wang, P.; Whangbo, M.-H. Highly Efficient Photocatalyst: TiO_2 Microspheres Produced from TiO_2 Nanosheets with a High Percentage of Reactive {001} Facets. *Chem.—Eur. J.* **2009**, *15*, 12576−12579.
(15) Wu, N. Q.; Wang, J.; Tafen, D.; Wang, H.; Zheng, J. G.; Lewis, J. P.; Liu, X. G.; Leonard, S. S.; Manivannan, A. Shape-Enhanced Photocatalytic Activity of Single-Crystalline Anatase TiO_2 (101) Nanobelts. *J. Am. Chem. Soc.* **2010**, *132*, 6679−6685.
(16) Sun, W.; Zhou, S. X.; You, B.; Wu, L. M. Facile Fabrication and High Photoelectric Properties of Hierarchically Ordered Porous TiO_2. *Chem. Mater.* **2012**, *24*, 3800−3810.
(17) Kong, M.; Li, Y.; Chen, X.; Tian, T.; Fang, P.; Zheng, F.; Zhao, X. Tuning the Relative Concentration Ratio of Bulk Defects to Surface Defects in TiO_2 Nanocrystals Leads to High Photocatalytic Efficiency. *J. Am. Chem. Soc.* **2011**, *133*, 16414−16417.

DOI: 10.1021/am5085447
ACS Appl. Mater. Interfaces 2015, 7, 3754−3763

(18) Zuo, F.; Wang, L.; Wu, T.; Zhang, Z.; Borchardt, D.; Feng, P. Self-Doped Ti^{3+} Enhanced Photocatalyst for Hydrogen Production Under Visible Light. *J. Am. Chem. Soc.* **2010**, *132*, 11856−11857.
(19) Liu, L.; Chen, X. Titanium Dioxide Nanomaterials: Self-Structural Modifications. *Chem. Rev.* **2014**, *114*, 9890−9918.
(20) Xia, T.; Zhang, Y.; Murowchick, J.; Chen, X. Vacuum-Treated Titanium Dioxide Nanocrystals: Optical Properties, Surface Disorder, Oxygen Vacancy, and Photocatalytic Activities. *Catal. Today* **2014**, *225*, 2−9.
(21) Lu, Z.; Yip, C.-T.; Wang, L.; Huang, H.; Zhou, L. Hydrogenated TiO_2 Nanotube Arrays as High-Rate Anodes for Lithium-Ion Microbatteries. *ChemPlusChem.* **2012**, *77*, 991−1000.
(22) Naldoni, A.; Allieta, M.; Santangelo, S.; Marelli, M.; Fabbri, F.; Cappelli, S.; Bianchi, C. L.; Psaro, R.; Dal Santo, V. Effect of Nature and Location of Defects on Bandgap Narrowing in Black TiO_2 Nanoparticles. *J. Am. Chem. Soc.* **2012**, *134*, 7600−7603.
(23) Li, G. C.; Zhang, Z. H.; Peng, H. R.; Chen, K. Z. Mesoporous Hydrogenated TiO_2 Microspheres for High Rate Capability Lithium Ion Batteries. *RSC Adv.* **2013**, *3*, 11507−11510.
(24) Xia, T.; Chen, X. B. Revealing the Structural Properties of Hydrogenated Black TiO_2 Nanocrystals. *J. Mater. Chem. A* **2013**, *1*, 2983−2989.
(25) Liu, L.; Yu, P. Y.; Chen, X.; Mao, S. S.; Shen, D. Z. Hydrogenation and Disorder in Engineered Black TiO_2. *Phys. Rev. Lett.* **2013**, *111*, 065505∼1−5.
(26) Lu, J.; Dai, Y.; Jin, H.; Huang, B. Effective Increasing of Optical Absorption and Energy Conversion Efficiency of Anatase TiO_2 Nanocrystals by Hydrogenation. *Phys. Chem. Chem. Phys.* **2011**, *13*, 18063−18068.
(27) Chen, X.; Liu, L.; Yu, P. Y.; Mao, S. S. Increasing Solar Absorption for Photocatalysis with Black Hydrogenated Titanium Dioxide Nanocrystals. *Science* **2011**, *331*, 746−750.
(28) Pan, H.; Zhang, Y. W.; Shenoy, V. B.; Gao, H. J. Effects of H-, N-, and (H, N)-Doping on the Photocatalytic Activity of TiO_2. *J. Phys. Chem. C* **2011**, *115*, 12224−12231.
(29) Zheng, Z.; Huang, B.; Lu, J.; Wang, Z.; Qin, X.; Zhang, X.; Dai, Y.; Whangbo, M. H. Hydrogenated Titania: Synergy of Surface Modification and Morphology Improvement for Enhanced Photocatalytic Activity. *Chem. Commun.* **2012**, *48*, 5733−5735.
(30) Wang, Z.; Yang, C. Y.; Lin, T. Q.; Yin, H.; Chen, P.; Wan, D. Y.; Xu, F. F.; Huang, F. Q.; Lin, J. H.; Xie, X. M.; Jiang, M. H. H-Doped Black Titania with Very High Solar Absorption and Excellent Photocatalysis Enhanced by Localized Surface Plasmon Resonance. *Adv. Funct. Mater.* **2013**, *23*, 5444−5450.
(31) Chen, X.; Li, C.; Grätzel, M.; Kostecki, R.; Mao, S. S. Nanomaterials for Renewable Energy Production and Storage. *Chem. Soc. Rev.* **2012**, *41*, 7909−7937.
(32) Wang, G.; Wang, H.; Ling, Y.; Tang, Y.; Yang, X.; Fitzmorris, R. C.; Wang, C.; Zhang, J. Z.; Li, Y. Hydrogen-Treated TiO_2 Nanowire Arrays for Photoelectrochemical Water Splitting. *Nano Lett.* **2011**, *11*, 3026−3033.
(33) Xia, T.; Zhang, W.; Murowchick, J. B.; Liu, G.; Chen, X. B. A Facile Method to Improve the Photocatalytic and Lithium-Ion Rechargeable Battery Performance of TiO_2 Nanocrystals. *Adv. Energy Mater.* **2013**, *3*, 1516−1523.
(34) Zhang, Q.; Uchaker, E.; Candelaria, S. L.; Cao, G. Nanomaterials for Energy Conversion and Storage. *Chem. Soc. Rev.* **2013**, *42*, 3127−3171.
(35) Zhu, W. D.; Wang, C. W.; Chen, J. B.; Li, D. S.; Zhou, F.; Zhang, H. L. Enhanced Field Emission from Hydrogenated TiO_2 Nanotube Arrays. *Nanotechnology* **2012**, *23*, 455204∼1−6.
(36) Ling, Y. C.; Cooper, J. K.; Yang, Y.; Wang, G. M.; Munoz, L.; Wang, H. Y.; Zhang, J. Z.; Li, Y. Chemically Modified Titanium Oxide Nanostructures for Dye-Sensitized Solar Cells. *Nano Energy* **2013**, *2*, 1373−1382.
(37) He, H.; Yang, K.; Wang, N.; Luo, F.; Chen, H. Hydrogenated TiO_2 Film for Enhancing Photovoltaic Properties of Solar Cells and Self-Sensitized Effect. *J. Appl. Phys.* **2013**, *114*, 213505∼1−5.
(38) Li, S.; Qiu, J.; Ling, M.; Peng, F.; Wood, B.; Zhang, S. Photoelectrochemical characterization of hydrogenated TiO_2 nanotubes as photoanodes for sensing applications. *ACS Appl. Mater. Interfaces* **2013**, *5*, 11129−11135.
(39) Yu, J.; Yang, Y.; Fan, R.; Li, L.; Li, X. Rapid Electron Injection in Nitrogen and Fluorine Doped Flower-Like Anatase TiO_2 with {001} Dominated Facets and Dye Sensitized Solar Cells with a 52% Increase in Photocurrent. *J. Phys. Chem. C* **2014**, *118*, 8795−8802.
(40) Zhang, Q.; Gao, L.; Guo, J. Effects of Calcination on the Photocatalytic Properties of Nanosized TiO_2 Powders Prepared by $TiCl_4$ Hydrolysis. *Appl. Catal., B* **2000**, *26*, 207−215.
(41) Li, Y.; Fan, Y.; Chen, Y. A Novel Method for Preparation of Nanocrystalline Rutile TiO_2 Powders by Liquid Hydrolysis of $TiCl_4$. *J. Mater. Chem.* **2002**, *12*, 1387−1390.
(42) Park, N. G.; Kang, M. G.; Ryu, K. S.; Kim, K. M.; Chang, S. H. Photovoltaic Characteristics of Dye-Sensitized Surface-Modified Nanocrystalline SnO_2 Solar Cells. *J. Photochem. Photobiol., A* **2004**, *161*, 105−110.
(43) Zeng, L.; Song, W.; Li, M.; Zeng, D.; Xie, C. Catalytic Oxidation of Formaldehyde on Surface of $HTiO_2$/$HCTiO_2$ without Light Illumination at Room Temperature. *Appl. Catal., B* **2014**, *147*, 490−498.
(44) Li, Y.; Hwang, D.-S.; Lee, N. H.; Kim, S.-J. Synthesis and Characterization of Carbon-Doped Titania as an Artificial Solar Light Sensitive Photocatalyst. *Chem. Phys. Lett.* **2005**, *404*, 25−29.
(45) Tauc, J.; Grigorovici, R.; Vancu, A. Optical Properties and Electronic Structure of Amorphous Germanium. *Phys. Status Solidi B* **1966**, *15*, 627−637.
(46) Janotti, A.; Varley, J. B.; Rinke, P.; Umezawa, N.; Kresse, G.; Van de Walle, C. G. Hybrid Functional Studies of the Oxygen Vacancy in TiO_2. *Phys. Rev. B: Condens. Matter Mater. Phys.* **2010**, *81*, 085212∼1−7.
(47) Cronemeyer, D. Infrared Absorption of Reduced Rutile TiO_2 Single Crystals. *Phys. Rev.* **1959**, *113*, 1222−1226.
(48) Linsebigler, A. L.; Lu, G. Q.; Yates, J. T. Photocatalysis on TiO_2 Surfaces - Principles, Mechanisms, and Selected Results. *Chem. Rev.* **1995**, *95*, 735−758.
(49) Redmond, C.; Fitzmaurice, D. Spectroscopic Determination of Flatband Potentials for Polycrystalline TiO_2 Electrodes in Nonaqueous Solvents. *J. Phys. Chem.* **1993**, *97*, 1426−1430.
(50) Rothenberger, G.; Fitzmaurice, D.; Grätzel, M. Spectroscopy of Conduction Band Electrons in Transparent Metal Oxide Semiconductor Films: Optical Determination of the Fiatband Potential of Colloidal Titanium Dioxide Films. *J. Phys. Chem.* **1992**, *96*, 5983−5986.
(51) Fabregat-Santiago, F.; Garcia-Belmonte, G.; Bisquert, J.; Bogdanoff, P.; Zaban, A. Mott-Schottky Analysis of Nanoporous Semiconductor Electrodes in Dielectric State Deposited on SnO_2(F) Conducting Substrates. *J. Electrochem. Soc.* **2003**, *150*, E293−E298.
(52) Wang, Z. S.; Yamaguchi, T.; Sugihara, H.; Arakawa, H. Significant Efficiency Improvement of the Black Dye-Sensitized Solar Cell through Protonation of TiO_2 Films. *Langmuir* **2005**, *21*, 4272−4276.
(53) Liu, G.; Li, F.; Wang, D. W.; Tang, D. M.; Liu, C.; Ma, X.; Lu, G. Q.; Cheng, H. M. Electron Field Emission of a Nitrogen-Doped TiO_2 Nanotube Array. *Nanotechnology* **2008**, *19*, 025606∼1−6.
(54) Luber, E. J.; Buriak, J. M. Reporting Performance in Organic Photovoltaic Devices. *ACS Nano* **2013**, *7*, 4708−4714.
(55) Kang, S. H.; Lim, J.-W.; Kim, H. S.; Kim, J.-Y.; Chung, Y.-H.; Sung, Y.-E. Photo and Electrochemical Characteristics Dependent on the Phase Ratio of Nanocolumnar Structured TiO_2 Films by RF Magnetron Sputtering Technique. *Chem. Mater.* **2009**, *21*, 2777−2788.
(56) Bisquert, J. Theory of the Impedance of Electron Diffusion and Recombination in a Thin Layer. *J. Phys. Chem. B* **2002**, *106*, 325−333.
(57) Bisquert, J.; Zaban, A.; Greenshtein, M.; Mora-Sero, I. Determination of Rate Constants for Charge Transfer and the Distribution of Semiconductor and Electrolyte Eectronic Energy Levels in Dye-Sensitized Solar Cells by Open-Circuit Photovoltage Decay Method. *J. Am. Chem. Soc.* **2004**, *126*, 13550−13559.

DOI: 10.1021/am5085447
ACS Appl. Mater. Interfaces 2015, 7, 3754−3763

(58) Mukherjee, K.; Teng, T. H.; Jose, R.; Ramakrishna, S. Electron Transport in Electrospun TiO_2 Nanofiber Dye-Sensitized Solar Cells. *Appl. Phys. Lett.* **2009**, *95*, 012101−1−3.
(59) Trancik, J. E.; Barton, S. C.; Hone, J. Transparent and Catalytic Carbon Nanotube Films. *Nano Lett.* **2008**, *8*, 982−987.
(60) Song, J.; Yang, H. B.; Wang, X.; Khoo, S. Y.; Wong, C.; Liu, X.-W.; Li, C. M. Improved Utilization of Photogenerated Charge Using Fluorine-Doped TiO_2 Hollow Spheres Scattering Layer in Dye-Sensitized Solar Cells. *ACS Appl. Mater. Interfaces* **2012**, *4*, 3712−3717.
(61) Wang, Q.; Moser, J.-E.; Grätzel, M. Electrochemical Impedance Spectroscopic Analysis of Dye-Sensitized Solar Cells. *J. Phys. Chem. B* **2005**, *109*, 14945−14953.
(62) Zhu, K.; Neale, N. R.; Miedaner, A.; Frank, A. J. Enhanced Charge-Collection Efficiencies and Light Scattering in Dye-Sensitized Solar Cells Using Oriented TiO_2 Nanotubes Arrays. *Nano Lett.* **2007**, *7*, 69−74.
(63) Zhu, K.; Vinzant, T. B.; Neale, N. R.; Frank, A. J. Removing Structural Disorder from Oriented TiO_2 Nanotube Arrays: Reducing the Dimensionality of Transport and Recombination in Dye-Sensitized Solar Cells. *Nano Lett.* **2007**, *7*, 3739−3746.
(64) Krülger, J.; Plass, R.; Grätzel, M.; Cameron, P. J.; Peter, L. M. Charge Transport and Back Reaction in Solid-State Dye-Sensitized Solar Cells: A Study Using Intensity-Modulated Photovoltage and Photocurrent Spectroscopy. *J. Phys. Chem. B* **2003**, *107*, 7536−7539.

DOI: 10.1021/am5085447
ACS Appl. Mater. Interfaces 2015, 7, 3754−3763